Testing the Organization of Whistler-mode Chorus Wave Properties by Plasmapause Location

David M. Malaspina[1,2], Allison N. Jaynes[3], Scot Elkington[2], Anthony Chan[4], George Hospodarsky[3], John Wygant[5]

[1]Department of Astrophysical and Planetary Sciences, University of Colorado, Boulder, Colorado, USA
[2]Laboratory for Atmospheric and Space Physics, University of Colorado, Boulder, Colorado, USA
[3]Department of Physics and Astronomy, University of Iowa, Iowa City, Iowa, USA
[4]Department of Physics and Astronomy, Rice University, Houston, Texas, USA
[5]School of Physics and Astronomy, University of Minnesota, Minneapolis, MN, USA

Key Points:

- An often-used assumption, that whistler-mode chorus properties are organized by L-shell, is tested and verified
- The plasmapause bounds whistler mode chorus activity but does not otherwise influence wave property distributions

Corresponding author: David Malaspina, `David.Malaspina@lasp.colorado.edu`

Abstract

Lower-band whistler-mode chorus waves are important to the dynamics of Earth's radiation belts, playing a key role in accelerating seed population electrons (100's of keV) to relativistic (> 1 MeV) energies, and in scattering electrons such that they precipitate into the atmosphere. When constructing and using statistical models of lower-band whistler-mode chorus wave power, it is commonly assumed that wave power is spatially distributed with respect to magnetic L-shell. At the same time, these waves are known to drop in power at the plasmapause, a cold plasma boundary which is dynamic in time and space relative to L-shell. This study organizes wave power and propagation direction data with respect to distance from the plasmapause location to evaluate what role the location of the plasmapause may play in defining the spatial distribution of lower band whistler-mode chorus wave power. It is found that characteristics of the statistical spatial distribution of equatorial lower band whistler mode chorus are determined by L-shell, and are largely independent of plasmapause location. The primary physical importance of the plasmapause is to act as an Earthward boundary to lower band whistler mode chorus wave activity. This behavior is consistent with an equatorial lower band whistler mode chorus wave power spatial distribution that follows the L-shell organization of the particles driving wave growth.

Plain Language Summary

Whistler-mode chorus are plasma waves that can efficiently accelerate particles in Earth's radiation belts, and act to scatter them out of the radiation belts into Earth's atmosphere. Models of the statistical behavior of these plasma waves are important for predicting the shape of the radiation belts. For decades, wave models relied on the assumption that these particular waves are distributed in space similar to radiation belt particles - by distance from Earth at the magnetic equator. Another possibility is that the spatial distribution of these waves could be modified by the location of Earth's cold plasma torus, the plasmasphere. The plasmasphere moves toward and away from Earth on different time scales than radiation belt particles. This study tests how whistler-mode chorus plasma waves are organized in space, by comparing statistics of plasma wave properties organized by distance from the Earth at the magnetic equator with the same data organized by distance from the plasmasphere outer boundary. The long-standing assumption is found to be valid. This result is consistent with the interpretation that the spatial distribution of the plasma waves under study is determined by the spatial organization of the particles that drive the wave growth.

1 Introduction

Whistler-mode chorus waves are important to the dynamics of the Earth's radiation belts, playing a key role in accelerating seed population electrons (100's of keV) to relativistic (> 1 MeV) energies, (e.g. (Horne & Thorne, 1998; Summers et al., 1998; Horne et al., 2005; Reeves et al., 2013; Jaynes et al., 2015)) and in scattering electrons across a broad range of energies, often leading to their precipitation into the atmosphere (e.g. (Shprits et al., 2008; Thorne, 2010; Kasahara et al., 2018)).

In the inner terrestrial magnetosphere, whistler-mode chorus waves appear in two bands, a lower band ($0.1f_{ce} < f < 0.5f_{ce}$), and an upper band, ($0.5f_{ce} < f < f_{ce}$), where f_{ce} is the electron cyclotron frequency (e.g. (Burtis & Helliwell, 1969; Tsurutani & Smith, 1977; Santolík et al., 2003)). Also, in this region, whistler-mode chorus waves are driven by cyclotron resonance with electron distributions with strong perpendicular temperature anisotropy (Schriver et al., 2010; Li et al., 2010; Lee et al., 2014), generated as electrons are adiabatically transported Earthward via impulsive injections from the plasma sheet during geomagnetic storms and substorms (e.g. (Sazhin & Hayakawa, 1992)).

A large number of studies have examined the spatial distribution of whistler-mode chorus wave power as a function of L-shell, MLT, and geomagnetic indices, demonstrating that the highest mean wave amplitudes occur in the dawn sector (where injected electrons gradient-curvature drift about the Earth), near the equator (where the strongest adiabatic temperature anisotropy occurs), and at L-shells of ∼7 (e.g. (Tsurutani & Smith, 1977; Meredith et al., 2001, 2003; Bortnik et al., 2007; Cully et al., 2008; Li et al., 2009, 2010, 2011; Meredith et al., 2012; Li et al., 2016; O. V. Agapitov et al., 2015; Meredith et al., 2018)). Several of these studies have demonstrated, using case studies of individual plasmapause crossings, that the plasmapause (the outer boundary of the plasmasphere, the cold dense plasma torus about Earth) constitutes an Earthward boundary to chorus wave activity (e.g. (Meredith et al., 2001)). The drop off of whistler-mode chorus wave power at the plasmapause is starkly visible in statistical wave power studies when chorus wave power near the geomagnetic equator is organized by distance from the plasmapause (Malaspina et al., 2016).

While the drop in equatorial whistler-mode chorus wave power at the plasmapause is well documented by case study observations, nearly all statistical studies of the spatial distribution of whistler-mode chorus power use the plasmapause only as an inner boundary for the identification of whistler-mode chorus waves (e.g. (Meredith et al., 2012; Li et al., 2016)). In these studies, wave property statistics are parameterized by L-shell, MLT, and geomagnetic indices, effectively averaging over many plasmapause radial locations and 'smoothing away' the physical drop in whistler-mode wave power at the plasmapause. This smoothing effect can be particularly strong because the plasmapause is dynamic in time and space with respect to L-shell. Plasmapause location varies in time through a wide range of L-shells (2 - 7) as a function of geomagnetic conditions, MLT, and the time history of both the solar wind convection electric field and ionospheric refilling (Carpenter & Lemaire, 2004).

This raises a question: to what extent does the spatial distribution of near-equatorial whistler-mode chorus wave power depend upon the plasmapause location? For example, the above-referenced studies examining the spatial distribution of whistler-mode chorus wave power all report a gradual drop in lower band whistler-mode wave power Earthward of $L = 7$. Is this a physical feature of the chorus wave spatial distribution or an artifact of smoothing wave statistics over variable plasmapause locations?

For a different whistler-mode wave in the inner magnetosphere, plasmaspheric hiss, the shape, location, and density profile of the plasmasphere strongly determine the wave power spatial distribution (Malaspina et al., 2016, 2017, 2018). For hiss, wave power modulation by plasmaspheric structure is thought to be largely a consequence of wave refraction, which is highly sensitive to the distribution of cold plasma density ((Maxworth & Gołkowski, 2017) and references therein). In contrast, the whistler-mode chorus source region and typical propagation regions are in general well outside the plasmapause (Bortnik et al., 2006; Chen et al., 2013), so the plasmasphere may have a weaker effect on chorus wave power distributions.

This work aims to quantify the impact of plasmapause location on the spatial distribution of near-equatorial lower band whistler-mode chorus wave properties. To do so, observations of whistler-mode chorus wave properties are compiled and organized by the location of the plasmapause with respect to Earth (L_{pp}), distance from the plasmapause (ΔL_{pp}), and magnetic local time (MLT). These statistics are then compared against wave property statistics organized using L-shell, L_{pp}, and MLT. In this study, the wave data are not explicitly parameterized by geomagnetic indices, though the geomagnetic activity level is implicitly included through L_{pp}.

Quasi-linear diffusion models of radiation belt dynamics typically ingest statistical models of wave power organized by L-shell, geomagnetic indices, and MLT (Subbotin & Shprits, 2009; Fok et al., 2011; Horne et al., 2013; Orlova et al., 2014; Glauert et al.,

2014). This work quantitatively tests an assumption commonly used in these models: that parameterization by L-shell is the most physically appropriate description of the chorus wave spatial distribution.

2 Data Set and Processing

This work uses data from the Van Allen Probes mission. These twin spacecraft were launched in August of 2012 and were de-orbited in 2019. During their mission, they orbited Earth between 600 km altitude and ∼6 Earth radii. They were spin stabilized, rotating once every ∼11 s, orbiting Earth every ∼9 hours, and precessing through all local times every ∼ 2 years. Their orbits covered ±20° of the magnetic equator. The instruments used in this analysis are the Electric and Magnetic Field Instrument Suite and Integrated Science (EMFISIS) (Kletzing et al., 2013) and the Electric Fields and Waves (EFW) instrument (Wygant et al., 2013).

This work examines lower band whistler-mode chorus wave power, wave normal angle, and Poynting flux direction as a function of parameters including: spacecraft L-shell location (L), distance between the spacecraft and the plasmapause in units of L-shell (ΔL_{pp}), and the distance of the plasmapause from Earth (L_{pp}).

The TS04D magnetic field model (Tsyganenko & Sitnov, 2005) is used to define L, ΔL_{pp}, and L_{pp} for each wave power observation. The specific L definition used here is McIlwain L-shell (McIlwain, 1961) for 90 degree pitch angle particles. Cold plasma density is estimated using the spacecraft floating potential data calibrated each day against densities determined via the upper hybrid resonance line, as in (Malaspina et al., 2016). Following (Moldwin et al., 2002), plasmapause crossings are identified as the most Earthward sharp density gradient (more than 5x change in density over 0.5 L-shell) on a given inbound or outbound pass of the spacecraft. The quantity ΔL_{pp} is defined as L - L_{pp}, where L_{pp} is the plasmapause location determined on a given outbound or inbound pass of the spacecraft. Data from passes without an identified plasmapause crossing are excluded in this work.

Wave power is determined using the EMFISIS survey power spectra of signals from the three search coil magnetometer (SCM) axes, as calculated on-board. These on-board calculated spectra capture 0.5 seconds of data every 6 seconds, producing power spectral densities between ∼2 Hz and ∼12 kHz in 65 pseudo-logarithmically spaced frequency bins. Lower-band whistler-mode chorus wave power for a given spectra is determined by summing the power spectral densities from all three SCM axes, multiplying by the bandwidth of each frequency bin, and summing data from $0.1 f_{ce}$ to $0.5 f_{ce}$. Here f_{ce} is the electron cyclotron frequency local to each spectral observation, determined using the magnetic field magnitude as measured by the fluxgate magnetometer.

Using SCM wave power data for this study instead of electric field wave data avoids complications associated with nonlinear electrostatic structure wave power in whistler-mode frequency bands (Mozer et al., 2013) as well as those associated with non-uniform sensor response along different measurement axes (Hartley et al., 2016). In SCM data, whistler-mode chorus are well-isolated narrow band (on a logarithmic scale) waves. Spectral bins dominated by magnetosonic waves are excluded using the following criteria on compressibility: $B_{\parallel}$ / $B_{\perp} < 0.6$. Here, $B_{\parallel}$ is the magnetic field wave amplitude parallel to the background magnetic field and $B_{\perp}$ is the magnetic field wave amplitude perpendicular to the background magnetic field, in a given spectral frequency bin. Data recorded during times of strong spacecraft charging, eclipse, and thruster firings are excluded from consideration. Data where the signal to noise ratio was less than 5 were excluded from consideration, where the SCM noise level definition from (Malaspina et al., 2017) was used.

This study also makes use of wave normal direction and Poynting flux direction for lower band whistler-mode chorus. Both quantities are derived from EMFISIS on-board cross-spectral data. Specifically examined in this study are (i) θ_{kB}, the polar angle between the wave normal vector direction and the background magnetic field, and (ii) θ_{SB}, the polar angle between the Poynting flux direction and the background magnetic field. Valid θ_{kB} values range from 0 (parallel/anti-parallel with $\vec{B}$) to 90 (perpendicular to $\vec{B}$). Valid θ_{SB} values range from 0 (parallel to $\vec{B}$) to 180 (anti-parallel to $\vec{B}$). θ_{kB} angles are calculated using the single value decomposition (SVD) analysis method (Santolík et al., 2003) applied to only the three axis SCM wave data. SVD-method wave normal angle determination was considered to be valid for frequency/time bins with planarity > 0.5, ellipticity > 0.5 and coherence between the two SCM signals orthogonal to the background magnetic field > 0.5. These quantities and their derivations are detailed in (Santolík et al., 2003).

The lower band whistler-mode chorus wave band can only be fully captured when 0.5 f_{ce} is below the upper frequency limit of the EMFISIS on-board power spectra (12 kHz). This condition is generally satisfied for $L > 3.5$. Closer to Earth than $L = 3.5$, prior studies indicate (e.g. (Meredith et al., 2018) and references therein), that lower band whistler-mode chorus wave power near the magnetic equator is often negligibly small, though this condition can be violated during periods of high geomagnetic activity. Lower band whistler-mode chorus wave power Earthward of the plasmapause, near the magnetic equator, is considered to be negligible in this study.

Data recorded by the Van Allen Probes between October 1, 2012 and March 31, 2018 were used in this study, encompassing nearly three full precessions of the orbit through all local times. Data from Van Allen Probe A after May of 2016 were not used because, in approximately June of 2016, radiation damage to preamplifier electronics degraded the spacecraft potential measurement on Van Allen Probe A to the point where it was not useful for density determination.

2.1 Analysis

Figure 1 shows data from one orbit of Van Allen Probe B on 01 September, 2014 when the orbit apogee was near dawn. Figure 1a shows the derived cold plasma density, with vertical red dashed lines indicating the identified plasmapause crossings on the inbound and outbound legs of the orbit. Between 14:00 and 16:00 UTC, a weak spacecraft charging event influenced the plasma density estimate. Figure 1b shows the total power spectral density from the two components of the electric field measured in the spacecraft spin plane. The frequencies 0.5 f_{ce} and 0.1 f_{ce} are overlaid in white solid lines, f_{ce} is shown as a dashed white line. Broadband signals corresponding to kinetic electric field structures such as phase space holes and kinetic Alfvén waves pervade the electric field wave data (Mozer et al., 2013; Chaston et al., 2015), especially near 11:00 and 15:00 UTC. Figure 1c shows the total power spectral density from all three SCM axes. Plasmaspheric hiss is observed Earthward of the plasmapause on both legs of the orbit, between ∼150 Hz and 2 kHz on the outbound leg and between ∼50 Hz and 2 kHz on the inbound leg. Figure 1d shows the band-integrated (0.1 f_{ce} to 0.5 f_{ce}) lower-band whistler-mode magnetic field wave power. Lower-band whistler-mode wave power is located outside the plasmasphere, between 0.1 f_{ce} and 0.5 f_{ce}, and is well-separated in frequency from other wave modes in the SCM data. While the lower-band whistler-mode waves show extended periods of activity, the variation in wave power during those periods can be as high as four orders of magnitude. This behavior is typical of whistler mode chorus (Santolík et al., 2010, 2014).

To compare lower-band whistler-mode properties under L-shell parameterization with those same properties under ΔL_{pp} parameterization, statistics of wave power, θ_{kB}, and θ_{SB} are presented. The full data set, after the exclusions described in the prior sec-

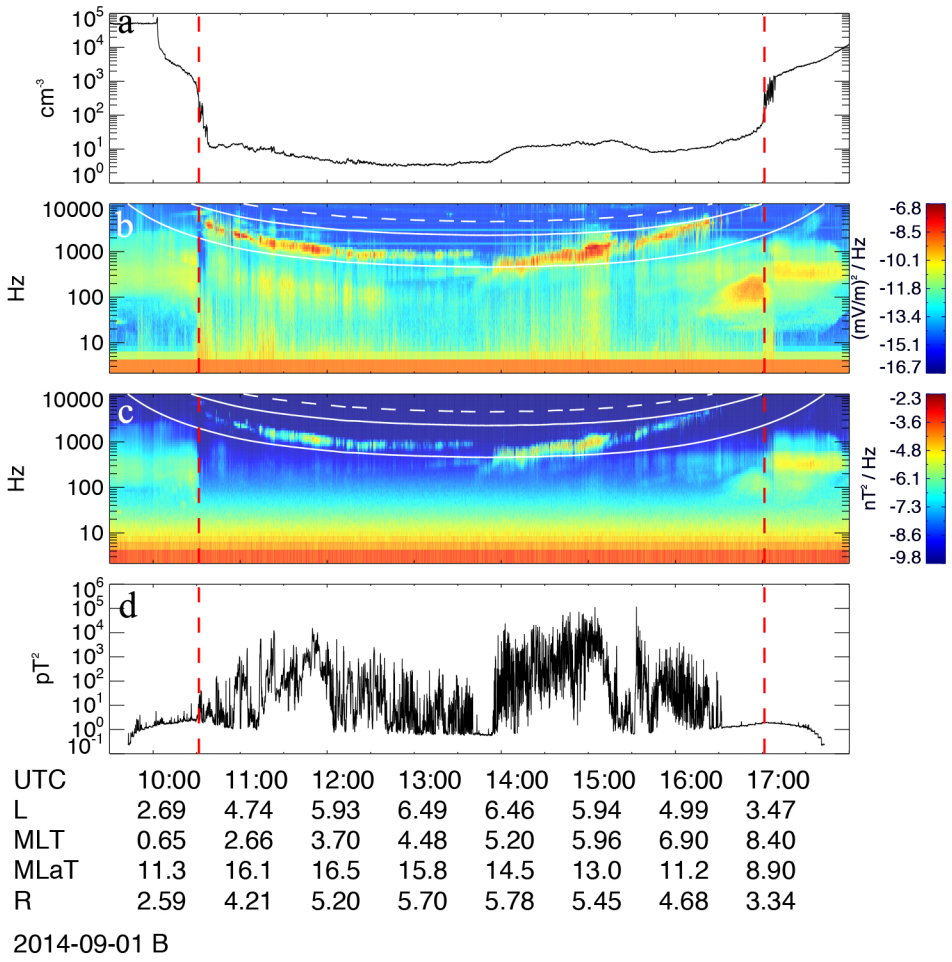

Figure 1. Plasma waves and density variation during one orbit of Van Allen Probe B on 01 September, 2014. (a) Plasma density derived from the spacecraft floating potential calibrated against the upper hybrid resonance line, (b) spectrogram of electric field wave power, (c) spectrogram of magnetic field wave power, (d) band-integrated wave power during this interval between 0.1 and 0.5 times the electron cyclotron frequency. Dashed white lines in (b) and (c) indicate the electron cyclotron frequency (f_{ce}) and solid white lines indicate $0.5f_{ce}$ and $0.1f_{ce}$.

tion, consists of $\sim 3.12 \times 10^7$ 0.5 s samples of lower-band whistler-mode waves distributed across L-shell, MLT, and geomagnetic activity level.

Wave property statistics are divided into four MLT sectors: Dawn ($3 < MLT < 9$), Noon ($9 < MLT < 15$), Dusk ($15 < MLT < 21$), and Midnight ($21 < MLT < 24$ and $0 < MLT < 3$). The statistics are also divided into four bins based on the location of the plasmapause with respect to Earth: $2 < L_{pp} < 3$, $3 < L_{pp} < 4$, $4 < L_{pp} < 5$, and $5 < L_{pp} < 6$. The geomagnetic activity level is convolved with this binning, as heavily eroded plasmaspheres occur when geomagnetic activity is high, and extended plasmaspheres occur when geomagnetic activity is low.

Figure 2 shows histograms of lower-band whistler-mode wave occurrence as a function of wave power and L-shell for data recorded in the Dawn sector ($3 < MLT < 9$). Plots in the left column show data organized by L-shell, while plots in the right column

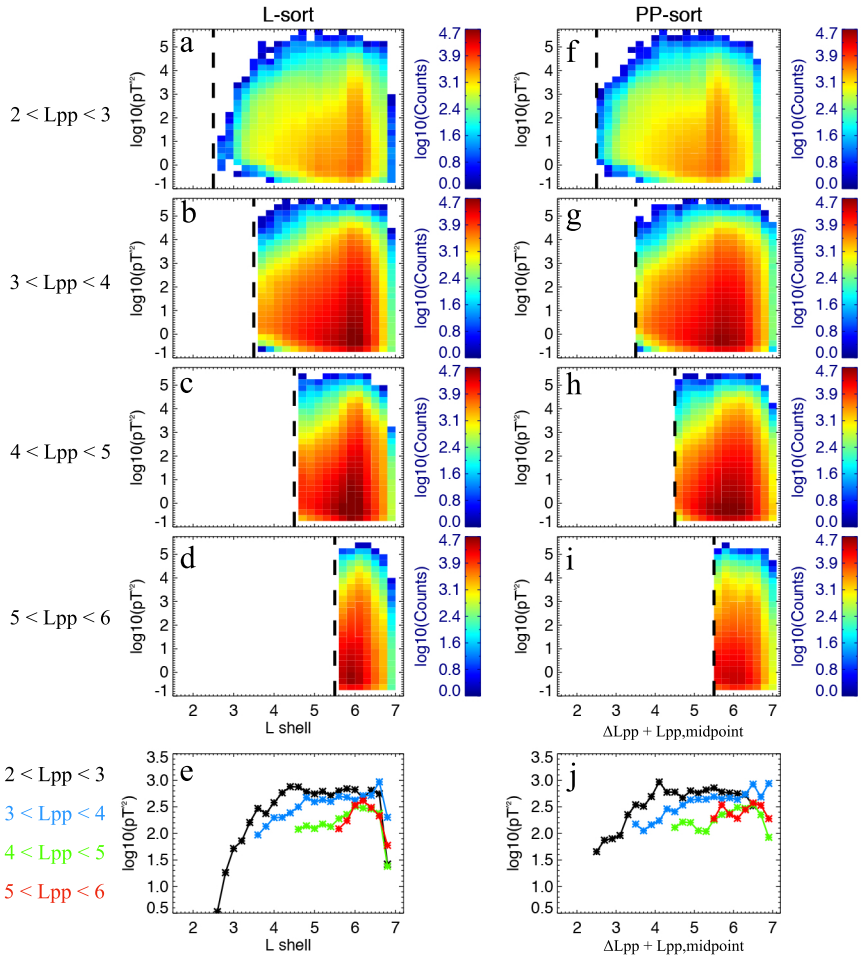

Figure 2. Histograms of lower-band whistler-mode wave occurrence as a function of wave power and L-shell for (a,b,c,d) data organized by L-shell and (f,g,h,i) data organized by distance to the plasmapause, shifted by the midpoint plasmapause location ($\Delta L_{pp} + L_{pp,midpoint}$), so that the data are directly comparable to (a,b,c,d). (a,f) data for plasmapause locations between $L = 2$ and $L = 3$, (b,g) data for plasmapause locations between $L = 3$ and $L = 4$, (c,h) data for plasmapause locations between $L = 4$ and $L = 5$,(d,i) data for plasmapause locations between $L = 5$ and $L = 6$. (e,j) Mean wave power as a function of L-shell derived from the distributions in (a,b,c,d) and (f,g,h,i).

show data organized by distance from the plasmapause, shifted by the value of L_{pp} at the midpoint of the plasmapause location bin ($L_{pp,midpoint} = 2.5, 3.5, 4.5$, etc.). This shift enables the plasmapause-sorted data to be directly compared with the L-sort data. The top row shows data where $2 < L_{pp} < 3$, the second row data where $3 < L_{pp} < 4$, the third row data where $4 < L_{pp} < 5$, and the fourth row data where $5 < L_{pp} < 6$. In each case, $L_{pp,midpoint}$ is indicated by a vertical dashed black line.

We choose not to collapse over the wave amplitude dimension when displaying these statistics because whistler-mode chorus wave amplitude distributions are known to be heavily tailed (Watt et al., 2017), with the probability of observing a particular amplitude decreasing toward higher amplitudes.

The bottom row shows the mean wave power per L-shell bin for each L_{pp} condition: black = $2 < L_{pp} < 3$, blue = $3 < L_{pp} < 4$, green = $4 < L_{pp} < 5$, and red = $5 < L_{pp} < 6$. While taking the mean collapses the amplitude dimension, mean wave power is often the most relevant quantity for quasi-linear representations of radiation belt modeling (Subbotin & Shprits, 2009; Fok et al., 2011; Horne et al., 2013; Orlova et al., 2014; Glauert et al., 2014).

The most striking feature of Figure 2 is the strong similarity between the left and right columns. Independent of whether the data are organized by L-shell or ΔL_{pp}, the highest amplitude waves are most likely to occur near $L = 6$, and the likelihood of observing high amplitude waves falls toward Earth. This trend persists for all L_{pp} bins. The overall shape of the amplitude/L-shell wave power distribution remains the same as L_{pp} varies, for both the L-sorted data and the ΔL_{pp}-sorted data. The only impact of L_{pp} variation is to set the Earthward cutoff of an otherwise weakly changing (in L-shell) distribution.

The two panels in the bottom row show that the mean wave amplitudes drop toward Earth, and they drop as L_{pp} increases, consistent with an overall change in geomagnetic activity. The drop in mean wave power beyond $L \approx 6.5$ occurs because the Van Allen Probes' orbital apogee rarely exceeds this value and the statistical coverage of these high-L bins is poor. The data in Figure 2e and Figure 2j are compared directly in Figure 5.

Figure 3 has a similar format to Figure 2, except that the quantity examined is θ_{kB}, the angle between the SVD-determined wave normal vector and the background magnetic field vector. Two distinct populations are present, a quasi-field aligned population with $\theta_{kB} < 30^o$, and an oblique population with $50^o < \theta_{kB} < 80^o$. The two populations separate more distinctly closer to Earth, and merge for $5 < L < 6$, the distance where the strongest wave amplitudes also occur. The wave normal angles of lower-band whistler-mode waves in the radiation belt are often well-described in terms of cold plasma theory, and have been examined extensively in other works (e.g. (Hartley et al., 2015; Li et al., 2016; O. V. Agapitov et al., 2016)).

The bottom row shows the peak value of the θ_{kB} distributions as a function of L-shell for the portion of the distribution where $\theta_{kB} < 45^o$. The data in Figure 3e and Figure 3j are compared directly in Figure 5.

The feature of interest for this study is, again, how similar the L-sorted data (left column) are to the ΔL_{pp}-sorted data (right column). The spatial morphology of the θ_{kB} distributions exterior to the plasmapause appear to be approximately static in L-shell as the plasmapause location varies. The portions of the distribution Earthward of the plasmapause are removed in response to outward motion of the plasmapause.

Figure 4 has the same format as Figure 3, and the quantity examined is θ_{SB}, the angle between the wave Poynting vector and the background magnetic field vector.

One population approximately parallel to $\vec{B}$, and one population approximately anti-parallel to $\vec{B}$, are present. The two populations are separated at all distances from Earth, but least so for $5 < L < 6$, the distance where the strongest wave amplitudes also occur. The parallel and anti-parallel populations of whistler-mode chorus near the magnetic equator have been well-documented and interpreted as whistler-mode chorus moving away from a magnetic equator source region (e.g. (Santolík et al., 2005; O. Agapitov et al., 2010)). As with wave power and θ_{kB}, the θ_{SB} distributions are strongly similar between the L-sorted data and ΔL_{pp}-sorted data.

The bottom row shows the peak (most likely to be observed) θ_{SB} value as a function of L-shell for the portion of the distribution where $\theta_{SB} < 45^o$. The data in Figure 4e and Figure 4j are compared directly in Figure 5.

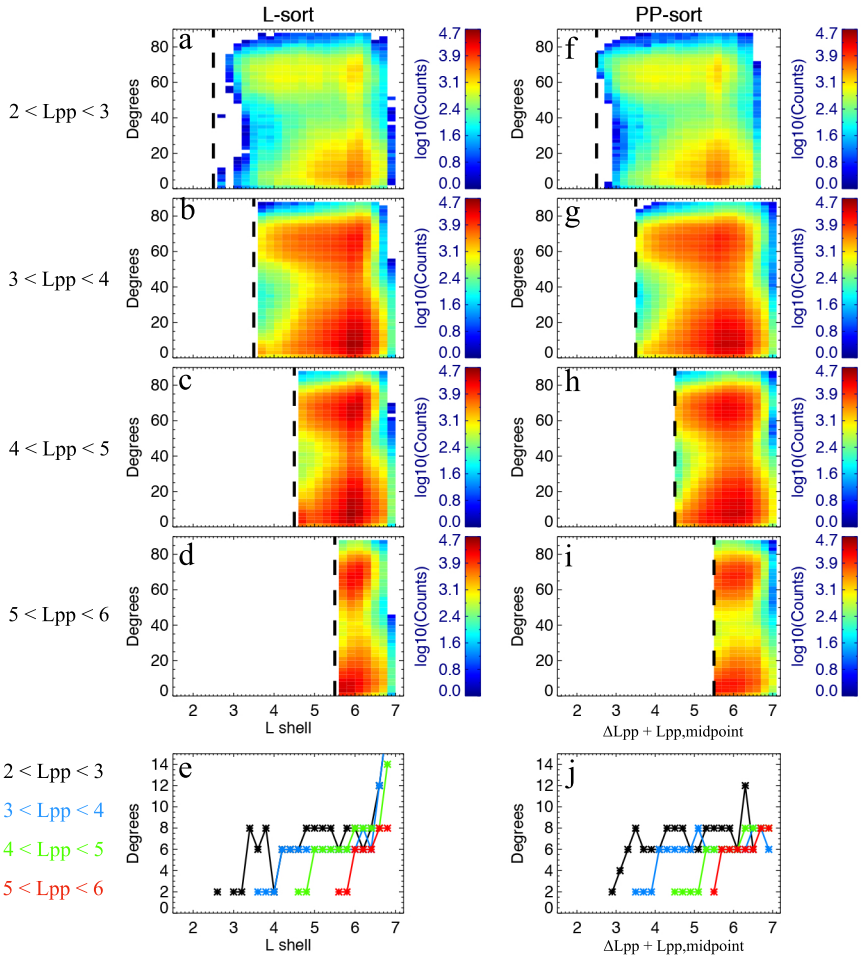

Figure 3. Same format as Figure 2, but for the quantity θ_{kB}. (e,j) Peak value of θ_{kB} for $\theta_{kB} < 45^o$ as a function of L-shell, for the distributions in (a,b,c,d) and (f,g,h,i).

Plots similar to Figure 2, Figure 3, and Figure 4, but for the other three quadrants (Noon, Dusk, Midnight) are included in the supplementary material. Each of these plots show the same behavior, in that (i) the L-shell and ΔL_{pp} distributions are strikingly similar, and (ii) the plasmapause acts to truncate the distribution toward Earth, but does not strongly influence other characteristics of the distribution (e.g. L-shell location of the largest amplitude waves).

3 Discussion

Figure 5 shows comparisons between the mean wave power (left column), peak θ_{kB} below 45^o (center column), and peak θ_{SB} below 45^o (right column) for L-sorted data (black traces) and ΔL_{pp}-sorted data (red traces, with x-axis of ΔL_{pp}+L$_{pp,midpoint}$). The four rows (top to bottom) show data for $2 < L_{pp} < 3$, $3 < L_{pp} < 4$, $4 < L_{pp} < 5$, and $5 < L_{pp} < 6$. These data are from the Dawn sector, and correspond to the data plotted in the bottom rows of Figures 2, 3, and 4. In all cases, there is close agreement between the L-sort and ΔL_{pp}-sort traces.

Small ($< 0.5L$) offsets are present, due to the $1L$ finite width of the L_{pp} bins. When translating the ΔL_{pp}-sorted data onto an L-shell-based x-axis, the bin-middle $L_{pp,midpoint}$

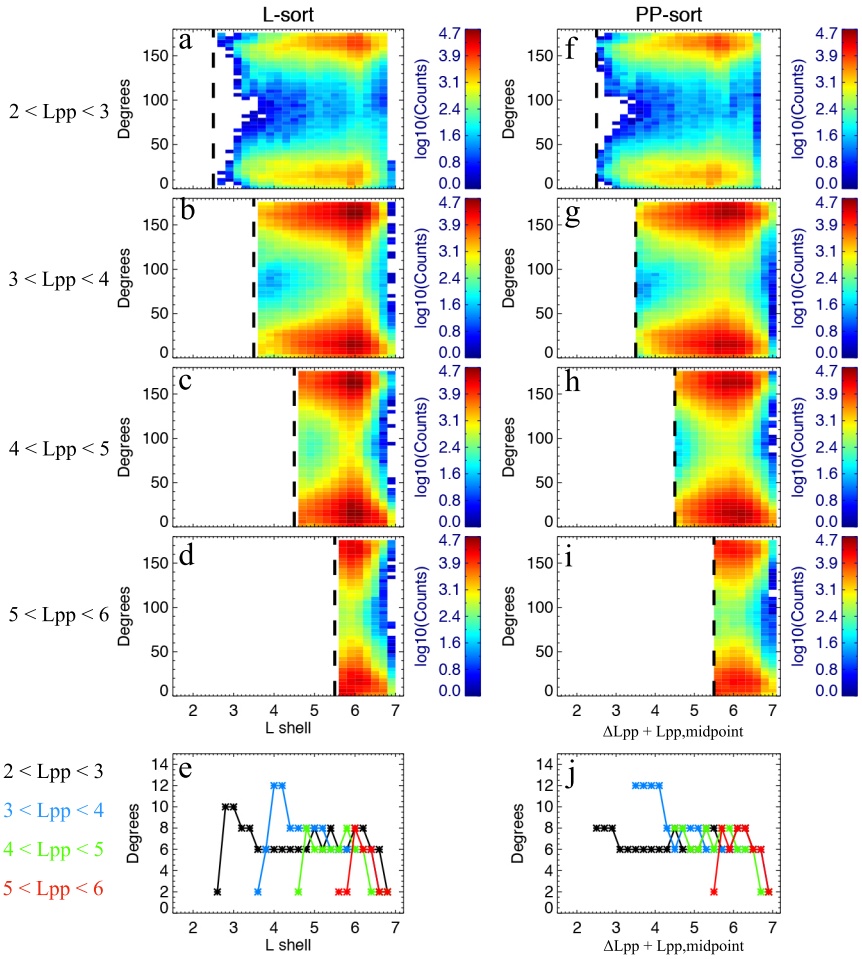

Figure 4. Same format as Figure 2, but for the quantity θ_{SB}. (e,j) Peak value of θ_{SB} for $\theta_{SB} < 45^o$ as a function of L-shell, for the distributions in (a,b,c,d) and (f,g,h,i).

value was used (e.g. $L_{pp,midpoint} = 2.5$ for $2 < L_{pp} < 3$). This can introduce a small offset in L-shell when the distribution of L_{pp} values in a given L_{pp} bin is skewed more toward the high end of the bin (as with $2 < L_{pp} < 3$).

The preceding analyses demonstrate that the distributions of lower band whistler mode chorus wave power, θ_{kB} and θ_{SB} retain a similar shape and spatial organization with respect to L-shell outside of the plasmapause, whether or not organization with respect to plasmapause position is considered. This is true even for locations close to the plasmapause. This result indicates that the primary role of the plasmapause in shaping the statistical spatial distribution of equatorial lower band whistler mode chorus wave properties is to define an Earthward boundary for wave activity.

This behavior is markedly different from plasmaspheric hiss, where the plasmaspheric density profile (Breneman et al., 2015; Malaspina et al., 2018) and plasmapause location (Malaspina et al., 2016) strongly determine the hiss wave power distribution. The differing behaviors of chorus and hiss spatial distributions are consistent with: (i) an equatorial lower band whistler mode chorus wave power spatial distribution that is co-located with the L-shell organization of particles driving wave growth (in agreement with prior studies such as (Li et al., 2010; Lee et al., 2014)) and, (ii) an equatorial plas-

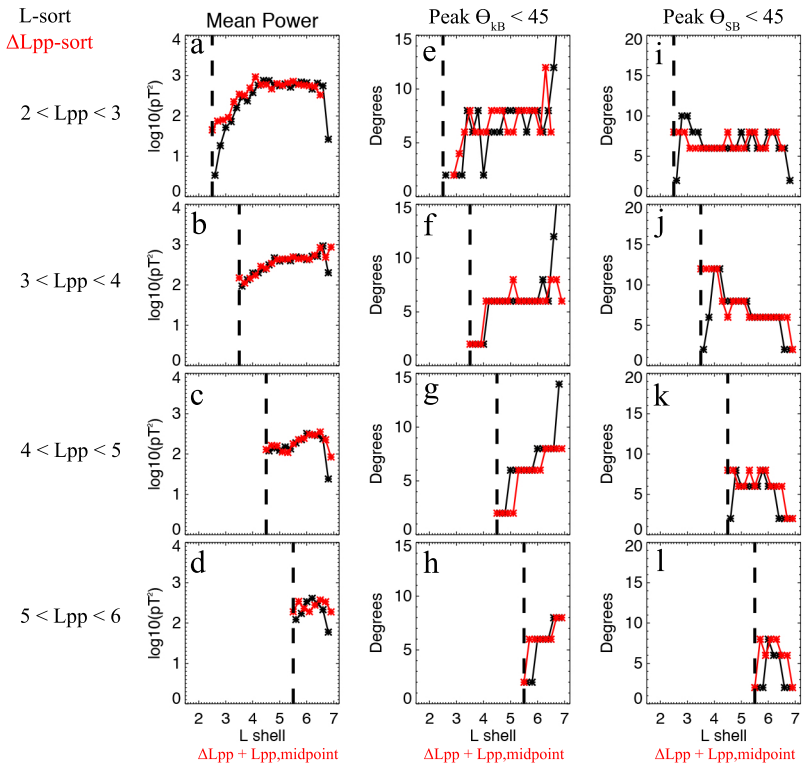

Figure 5. Comparison between wave mean power (left column), θ_{kB} (middle column), and θ_{SB} (right column) for L-sorted wave data (black traces) and $\Delta L_{pp} + L_{pp,midpoint}$-sorted data (red traces). (a,e,i) data for plasmapause locations between $L = 2$ and $L = 3$, (b,f,j) data for plasmapause locations between $L = 3$ and $L = 4$, (c,g,k) data for plasmapause locations between $L = 4$ and $L = 5$, (d,h,l) data for plasmapause locations between $L = 5$ and $L = 6$.

maspheric hiss wave power spatial distribution that is determined by whistler-mode propagation effects and consequently, the refractive properties of the plasma within the plasmasphere (Chen et al., 2012; Malaspina et al., 2018). One exception to this dichotomy is low frequency hiss ($< 150Hz$), which has been shown to be co-located with the particles driving its wave growth (Shi et al., 2017).

4 Conclusions

Understanding the spatial distribution of equatorial lower band whistler-mode chorus wave power statistically is important for our understanding of radiation belt dynamics, in that whistler-mode waves play a significant role in both relativistic electron acceleration and electron scattering. It is well-understood from prior observations that whistler-mode chorus wave power drops at the plasmapause, but the plasmapause is a dynamic boundary in both space and time with respect to L-shell.

The goal of this study was to compare statistical distributions of lower band whistler-mode chorus wave properties using L-shell sorting and plasmapause-based sorting of the data. The primary result is that the plasmapause location does not play a strong role in shaping the statistical spatial distribution of equatorial lower band whistler mode chorus outside of the plasmapause. In the Van Allen Probes data, whistler-mode chorus mean

wave amplitudes peak near the apogee of the Van Allen Probes orbit and fall Earthward of that location, regardless of whether the plasmapause location is considered.

The lack of systematic difference between the data when sorted by L-shell or by distance from the plasmapause supports the long-used assumption that equatorial lower band whistler mode chorus wave properties are physically organized by L-shell. Therefore, quasi-linear diffusion models of radiation belt dynamics are expected to produce similar results whether they use L-sorted data or plasmapause-sorted data for lower band whistler mode chorus waves.

Acknowledgments

The authors thank the Van Allen Probes team, especially the EFW and EMFISIS teams for their support. This work was funded by NASA award NNX17AI51G. All Van Allen Probes data used in this work are available from the EFW and EMFISIS team websites, which one can link to here: http://rbspgway.jhuapl.edu. The authors acknowledge the International Space Sciences Institute (ISSI) and the participants in a 2020 ISSI workshop in Bern.

References

Agapitov, O., Krasnoselskikh, V., Zaliznyak, Y., Angelopoulos, V., Le Contel, O., & Rolland, G. (2010, June). Chorus source region localization in the Earth's outer magnetosphere using THEMIS measurements. *Annales Geophysicae*, *28*(6), 1377-1386. doi: 10.5194/angeo-28-1377-2010

Agapitov, O. V., Artemyev, A. V., Mourenas, D., Mozer, F. S., & Krasnoselskikh, V. (2015, December). Empirical model of lower band chorus wave distribution in the outer radiation belt. *Journal of Geophysical Research (Space Physics)*, *120*, 10. doi: 10.1002/2015JA021829

Agapitov, O. V., Mourenas, D., Artemyev, A. V., & Mozer, F. S. (2016, November). Exclusion principle for very oblique and parallel lower band chorus waves. *Geophysical Research Letters*, *43*(21), 11,112-11,120. doi: 10.1002/2016GL071250

Bortnik, J., Inan, U. S., & Bell, T. F. (2006, February). Landau damping and resultant unidirectional propagation of chorus waves. *Geophysical Research Letters*, *33*, L03102. doi: 10.1029/2005GL024553

Bortnik, J., Thorne, R. M., & Meredith, N. P. (2007, August). Modeling the propagation characteristics of chorus using CRRES suprathermal electron fluxes. *Journal of Geophysical Research (Space Physics)*, *112*, A08204. doi: 10.1029/2006JA012237

Breneman, A. W., Halford, A., Millan, R., McCarthy, M., Fennell, J., Sample, J., ... Kletzing, C. A. (2015, July). Global-scale coherence modulation of radiation-belt electron loss from plasmaspheric hiss. *Nature*, *523*, 193-195. doi: 10.1038/nature14515

Burtis, W. J., & Helliwell, R. A. (1969). Banded chorus-A new type of VLF radiation observed in the magnetosphere by OGO 1 and OGO 3. *Journal of Geophysical Research*, *74*, 3002. doi: 10.1029/JA074i011p03002

Carpenter, D., & Lemaire, J. (2004, December). The Plasmasphere Boundary Layer. *Annales Geophysicae*, *22*, 4291-4298. doi: 10.5194/angeo-22-4291-2004

Chaston, C. C., Bonnell, J. W., Kletzing, C. A., Hospodarsky, G. B., Wygant, J. R., & Smith, C. W. (2015, October). Broadband low-frequency electromagnetic waves in the inner magnetosphere. *Journal of Geophysical Research (Space Physics)*, *120*, 8603-8615. doi: 10.1002/2015JA021690

Chen, L., Li, W., Bortnik, J., & Thorne, R. M. (2012, April). Amplification of whistler-mode hiss inside the plasmasphere. *Geophysical Review Letters*, *39*, L08111. doi: 10.1029/2012GL051488

Chen, L., Thorne, R. M., Li, W., & Bortnik, J. (2013, March). Modeling the wave normal distribution of chorus waves. *Journal of Geophysical Research (Space Physics)*, *118*, 1074-1088. doi: 10.1029/2012JA018343

Cully, C. M., Bonnell, J. W., & Ergun, R. E. (2008, June). THEMIS observations of long-lived regions of large-amplitude whistler waves in the inner magnetosphere. *Geophysical Research Letters*, *35*, L17S16. doi: 10.1029/2008GL033643

Fok, M.-C., Glocer, A., Zheng, Q., Horne, R. B., Meredith, N. P., Albert, J. M., & Nagai, T. (2011, July). Recent developments in the radiation belt environment model. *Journal of Atmospheric and Solar-Terrestrial Physics*, *73*, 1435-1443. doi: 10.1016/j.jastp.2010.09.033

Glauert, S. A., Horne, R. B., & Meredith, N. P. (2014, January). Three-dimensional electron radiation belt simulations using the BAS Radiation Belt Model with new diffusion models for chorus, plasmaspheric hiss, and lightning-generated whistlers. *Journal of Geophysical Research (Space Physics)*, *119*, 268-289. doi: 10.1002/2013JA019281

Hartley, D. P., Chen, Y., Kletzing, C. A., Denton, M. H., & Kurth, W. S. (2015, February). Applying the cold plasma dispersion relation to whistler mode chorus waves: EMFISIS wave measurements from the Van Allen Probes. *Journal of Geophysical Research (Space Physics)*, *120*(2), 1144-1152. doi: 10.1002/2014JA020808

Hartley, D. P., Kletzing, C. A., Kurth, W. S., Bounds, S. R., Averkamp, T. F., Hospodarsky, G. B., ... Watt, C. E. J. (2016, May). Using the cold plasma dispersion relation and whistler mode waves to quantify the antenna sheath impedance of the Van Allen Probes EFW instrument. *Journal of Geophysical Research (Space Physics)*, *121*, 4590-4606. doi: 10.1002/2016JA022501

Horne, R. B., Glauert, S. A., Meredith, N. P., Boscher, D., Maget, V., Heynderickx, D., & Pitchford, D. (2013, April). Space weather impacts on satellites and forecasting the Earth's electron radiation belts with SPACECAST. *Space Weather*, *11*, 169-186. doi: 10.1002/swe.20023

Horne, R. B., & Thorne, R. M. (1998). Potential waves for relativistic electron scattering and stochastic acceleration during magnetic storms. *Geophysical Research Letters*, *25*, 3011-3014. doi: 10.1029/98GL01002

Horne, R. B., Thorne, R. M., Shprits, Y. Y., Meredith, N. P., Glauert, S. A., Smith, A. J., ... Decreau, P. M. E. (2005, September). Wave acceleration of electrons in the Van Allen radiation belts. *Nature*, *437*, 227-230. doi: 10.1038/nature03939

Jaynes, A. N., Baker, D. N., Singer, H. J., Rodriguez, J. V., Loto'aniu, T. M., Ali, A. F., ... Reeves, G. D. (2015, September). Source and seed populations for relativistic electrons: Their roles in radiation belt changes. *Journal of Geophysical Research (Space Physics)*, *120*, 7240-7254. doi: 10.1002/2015JA021234

Kasahara, S., Miyoshi, Y., Yokota, S., Mitani, T., Kasahara, Y., Matsuda, S., ... Shinohara, I. (2018, February). Pulsating aurora from electron scattering by chorus waves. *Nature*, *554*, 337-340. doi: 10.1038/nature25505

Kletzing, C. A., Kurth, W. S., Acuna, M., MacDowall, R. J., Torbert, R. B., Averkamp, T., ... Tyler, J. (2013, November). The Electric and Magnetic Field Instrument Suite and Integrated Science (EMFISIS) on RBSP. *Space Science Reviews*, *179*, 127-181. doi: 10.1007/s11214-013-9993-6

Lee, D.-H., Lee, D.-Y., Shin, D.-K., Kim, J.-H., & Cho, J.-H. (2014, December). A Statistical Test of the Relationship Between Chorus Wave Activation and Anisotropy of Electron Phase Space Density. *Journal of Astronomy and Space Sciences*, *31*, 295-301. doi: 10.5140/JASS.2014.31.4.295

Li, W., Bortnik, J., Thorne, R. M., & Angelopoulos, V. (2011, December). Global distribution of wave amplitudes and wave normal angles of chorus waves using

THEMIS wave observations. *Journal of Geophysical Research (Space Physics)*, *116*, A12205. doi: 10.1029/2011JA017035

Li, W., Santolik, O., Bortnik, J., Thorne, R. M., Kletzing, C. A., Kurth, W. S., & Hospodarsky, G. B. (2016, May). New chorus wave properties near the equator from Van Allen Probes wave observations. *Geophysical Research Letters*, *43*, 4725-4735. doi: 10.1002/2016GL068780

Li, W., Thorne, R. M., Angelopoulos, V., Bortnik, J., Cully, C. M., Ni, B., ... Magnes, W. (2009, May). Global distribution of whistler-mode chorus waves observed on the THEMIS spacecraft. *Geophysical Research Letters*, *36*, L09104. doi: 10.1029/2009GL037595

Li, W., Thorne, R. M., Nishimura, Y., Bortnik, J., Angelopoulos, V., McFadden, J. P., ... Auster, U. (2010, June). THEMIS analysis of observed equatorial electron distributions responsible for the chorus excitation. *Journal of Geophysical Research (Space Physics)*, *115*, A00F11. doi: 10.1029/2009JA014845

Malaspina, D. M., Jaynes, A. N., Boulé, C., Bortnik, J., Thaller, S. A., Ergun, R. E., ... Wygant, J. R. (2016, August). The distribution of plasmaspheric hiss wave power with respect to plasmapause location. *Geophysical Review Letters*, *43*, 7878-7886. doi: 10.1002/2016GL069982

Malaspina, D. M., Jaynes, A. N., Hospodarsky, G., Bortnik, J., Ergun, R. E., & Wygant, J. (2017, August). Statistical properties of low-frequency plasmaspheric hiss. *Journal of Geophysical Research (Space Physics)*, *122*, 8340-8352. doi: 10.1002/2017JA024328

Malaspina, D. M., Ripoll, J.-F., Chu, X., Hospodarsky, G., & Wygant, J. (2018, September). Variation in Plasmaspheric Hiss Wave Power With Plasma Density. *Geophysical Research Letters*, *45*, 9417-9426. doi: 10.1029/2018GL078564

Maxworth, A. S., & Gołkowski, M. (2017, July). Magnetospheric whistler mode ray tracing in a warm background plasma with finite electron and ion temperature. *Journal of Geophysical Research (Space Physics)*, *122*, 7323-7335. doi: 10.1002/2016JA023546

McIlwain, C. E. (1961, November). Coordinates for Mapping the Distribution of Magnetically Trapped Particles. *Journal of Geophysical Research*, *66*, 3681-3691. doi: 10.1029/JZ066i011p03681

Meredith, N. P., Horne, R. B., & Anderson, R. R. (2001, July). Substorm dependence of chorus amplitudes: Implications for the acceleration of electrons to relativistic energies. *Journal of Geophysical Research*, *106*, 13165-13178. doi: 10.1029/2000JA900156

Meredith, N. P., Horne, R. B., Kersten, T., Li, W., Bortnik, J., Sicard, A., & Yearby, K. H. (2018, June). Global Model of Plasmaspheric Hiss From Multiple Satellite Observations. *Journal of Geophysical Research (Space Physics)*, *123*, 4526-4541. doi: 10.1029/2018JA025226

Meredith, N. P., Horne, R. B., Sicard-Piet, A., Boscher, D., Yearby, K. H., Li, W., & Thorne, R. M. (2012, October). Global model of lower band and upper band chorus from multiple satellite observations. *Journal of Geophysical Research (Space Physics)*, *117*, A10225. doi: 10.1029/2012JA017978

Meredith, N. P., Horne, R. B., Thorne, R. M., & Anderson, R. R. (2003, August). Favored regions for chorus-driven electron acceleration to relativistic energies in the Earth's outer radiation belt. *Geophysical Research Letters*, *30*, 1871. doi: 10.1029/2003GL017698

Moldwin, M. B., Downward, L., Rassoul, H. K., Amin, R., & Anderson, R. R. (2002, November). A new model of the location of the plasmapause: CRRES results. *Journal of Geophysical Research (Space Physics)*, *107*, 1339. doi: 10.1029/2001JA009211

Mozer, F. S., Bale, S. D., Bonnell, J. W., Chaston, C. C., Roth, I., & Wygant, J. (2013, December). Megavolt Parallel Potentials Arising from Double-

Layer Streams in the Earth's Outer Radiation Belt. *Physical Review Letters*, *111*(23), 235002. doi: 10.1103/PhysRevLett.111.235002

Orlova, K., Spasojevic, M., & Shprits, Y. (2014, June). Activity-dependent global model of electron loss inside the plasmasphere. *Geophysical Review Letters*, *41*, 3744-3751. doi: 10.1002/2014GL060100

Reeves, G., Spence, H. E., Henderson, M. G., Friedel, R. H. W., Funsten, H. O., Baker, D. N., ... Morley, S. K. (2013, August). Electron Acceleration in the Heart of the Van Allen Radiation Belts. *Science*, *341*, 991-994. doi: 10.1126/science.1237743

Santolík, O., Gurnett, D. A., Pickett, J. S., Grimald, S., Décreau, P. M. E., Parrot, M., ... Fazakerley, A. (2010, August). Wave-particle interactions in the equatorial source region of whistler-mode emissions. *Journal of Geophysical Research (Space Physics)*, *115*, A00F16. doi: 10.1029/2009JA015218

Santolík, O., Gurnett, D. A., Pickett, J. S., Parrot, M., & Cornilleau-Wehrlin, N. (2003, July). Spatio-temporal structure of storm-time chorus. *Journal of Geophysical Research (Space Physics)*, *108*, 1278. doi: 10.1029/2002JA009791

Santolík, O., Gurnett, D. A., Pickett, J. S., Parrot, M., & Cornilleau-Wehrlin, N. (2005, January). Central position of the source region of storm-time chorus. *Planetary and Space Sciences*, *53*(1-3), 299-305. doi: 10.1016/j.pss.2004.09.056

Santolík, O., Macúšová, E., Kolmašová, I., Cornilleau-Wehrlin, N., & Conchy, Y. (2014, April). Propagation of lower-band whistler-mode waves in the outer Van Allen belt: Systematic analysis of 11 years of multi-component data from the Cluster spacecraft. *Geophysical Research Letters*, *41*, 2729-2737. doi: 10.1002/2014GL059815

Sazhin, S. S., & Hayakawa, M. (1992, May). Magnetospheric chorus emissions - A review. *Planetary and Space Science*, *40*, 681-697. doi: 10.1016/0032-0633(92)90009-D

Schriver, D., Ashour-Abdalla, M., Coroniti, F. V., LeBoeuf, J. N., Decyk, V., Travnicek, P., ... Fazakerley, A. N. (2010, August). Generation of whistler mode emissions in the inner magnetosphere: An event study. *Journal of Geophysical Research (Space Physics)*, *115*, A00F17. doi: 10.1029/2009JA014932

Shi, R., Li, W., Ma, Q., Reeves, G. D., Kletzing, C. A., Kurth, W. S., ... Claudepierre, S. G. (2017, October). Systematic Evaluation of Low-Frequency Hiss and Energetic Electron Injections. *Journal of Geophysical Research (Space Physics)*, *122*, 10. doi: 10.1002/2017JA024571

Shprits, Y. Y., Subbotin, D. A., Meredith, N. P., & Elkington, S. R. (2008, November). Review of modeling of losses and sources of relativistic electrons in the outer radiation belt II: Local acceleration and loss. *Journal of Atmospheric and Solar-Terrestrial Physics*, *70*, 1694-1713. doi: 10.1016/j.jastp.2008.06.014

Subbotin, D. A., & Shprits, Y. Y. (2009, October). Three-dimensional modeling of the radiation belts using the Versatile Electron Radiation Belt (VERB) code. *Space Weather*, *7*, S10001. doi: 10.1029/2008SW000452

Summers, D., Thorne, R. M., & Xiao, F. (1998, September). Relativistic theory of wave-particle resonant diffusion with application to electron acceleration in the magnetosphere. *Journal of Geophysical Research*, *103*, 20487-20500. doi: 10.1029/98JA01740

Thorne, R. M. (2010, November). Radiation belt dynamics: The importance of wave-particle interactions. *Geophysical Review Letters*, *37*, 22107. doi: 10.1029/2010GL044990

Tsurutani, B. T., & Smith, E. J. (1977, November). Two types of magnetospheric ELF chorus and their substorm dependences. *Journal of Geophysical Research*, *82*, 5112-5128. doi: 10.1029/JA082i032p05112

Tsyganenko, N. A., & Sitnov, M. I. (2005, March). Modeling the dynamics of the inner magnetosphere during strong geomagnetic storms. *Journal of Geophysical*

Research (Space Physics), *110*, A03208. doi: 10.1029/2004JA010798

Watt, C. E. J., Rae, I. J., Murphy, K. R., Anekallu, C., Bentley, S. N., & Forsyth, C. (2017, September). The parameterization of wave-particle interactions in the Outer Radiation Belt. *Journal of Geophysical Research (Space Physics)*, *122*, 9545-9551. doi: 10.1002/2017JA024339

Wygant, J. R., Bonnell, J. W., Goetz, K., Ergun, R. E., Mozer, F. S., Bale, S. D., ... Tao, J. B. (2013, November). The Electric Field and Waves Instruments on the Radiation Belt Storm Probes Mission. *Space Science Reviews*, *179*, 183-220. doi: 10.1007/s11214-013-0013-7